

A Seven Link Biped Robot Walking Pattern Generation On Various Surfaces

MOHAMMADREZA RANJBAR, RENE V. MAYORGA

Wise & Intelligent Systems & Entities (W.I.S.E) Lab

Faculty of Engineering and Applied Science

University of Regina

3737 Wascana Parkway, Regina, SK, S4S 0A2

CANADA

ranjbamo@uregina.ca Rene.Mayorga@uregina.ca

Abstract: This Paper presents a periodic approach with scalable walking trajectory based on gait characteristic parameters including length, maximum height and time cycle. The proposed methodology is split in two parts: robot trajectory and dynamic stability examination. The lower body is in charge of general bipedal walking trajectory where a limited number of breakpoints in both stable and unstable phases are identified. Consequently, three joints (hip, knee and ankle) positions are derived for a seven link biped robot. Considering the fields of Computational Intelligence and Soft Computing leads to an efficient non-conventional approach to generate a smooth walking trajectory. The methodology for walking pattern planning based on Artificial Neural Networks using Radial Basis Function intends to fit a curve on derived breakpoints. The biped robot stability during walking cycles is investigated by the Zero Moment Point (ZMP) criterion. For the dynamic stability study, the ZMP for a stable condition in a determined polygon of support in every single gait step is calculated. For trunk motion adjustment and lower limb movement compensation, a Linear Inverted Pendulum model and ZMP criterion are employed to obtain upper body trajectory satisfying whole robot walking dynamic stability.

Key-Words: Neural Networks, Radial Basis Functions, Bipedal Robot Walking, Trajectory Planning

1 Introduction

In recent years, dynamic bipedal walking and in general legged locomotion have inspired growing interests. The reason is partly the demand for robots enabled to operate in human oriented environments. Biped robot structure allows the body to travel along a different trajectory than the feet such that the whole body walking pattern is smooth, despite the roughness of the environment. As the applications are widespread, reasons to analyze and derive counterpart models of human being behavior in real life sound persuasive. There is a huge amount of potential applications in patients' mobility, rehabilitation, and video games industries which could benefit from a reliable humanoid robot walking method. The starting point for biped robot locomotion is using an efficient method of trajectory planning. Ideally, it is featured with a simple implementation and fast calculation in addition to compatibility with real time applications. Moreover, the proposed trajectory implementation needs to intake input parameters such as gait length, gait time period and maximum foot height to facilitate manipulating the speed and position of the robot's joints. A significant number of efforts focus on bipedal walking development in both real and virtual environments. Generally, approaches to

bipedal walking concern with two major issues: kinematic smoothness and dynamic balance. Kinematics describes motion of joints, linkages and whole body of the robot without consideration of the causes of the motion. However, Dynamics is studying of forces and torques and their effects on motion.

Motion data obtained from either motion capture or manual calculation are Kinematics techniques basis. Respectively, derived points of motion are interpolated in order to build a motion trajectory. This method gives smooth and continuous walking pattern that might be different from the original input sequences. This method of locomotion appropriately responds to input parameters justifications, and follows desired paths through different environments with obstacles avoidance capability. In this study, Inverse Kinematics (IK) provides a computation tool for manual calculations of joints positions on a Cartesian plane to locate biped linkages as desired. Bipedal Motion is inherently unstable; hence, to control locomotion skills the first objective is to balance maintenance. Balance is categorized as static or dynamic. In static balance, the projection of the Center of Mass (COM) on the ground is always kept within the support area of stance feet. COM within area of

support results in stable gaits but a very low walking speed [1]. Static balance disadvantages led researchers to dynamic walking methods [2,3]. Zero Moment Point algorithm suggested by Vukobratović [4] is one of the most popular dynamic bipedal walking methods. The algorithm has evolved since it was first proposed and been utilized in numerous full-sized humanoid robots for walking purposes. In Dynamic balance, ZMP is retained within the margin of support polygon. This approach makes faster gaits than static balance; but, disturbances may easily tip over a biped robot.

Stable walking pattern synthesis received many researchers' attentions. Huang et al [5] efficiently identified key points and foot motion parameters constraints in single and double support phases of gait cycles. Consequently, constraints formulation led to an adaptive foot trajectory generation by third spline periodic interpolation. They then applied an iterative computation to derive the hip trajectory by formulating the problem of the smooth hip motion with the largest stability margin. In this approach, the trunk of body is considered in parallel with Z axis in gait cycles. A similar approach has been utilized by Mousavi et al [6,7] for various surfaces and combined paths. Fattah et al [8] presented a simplified comparable method by keeping hip joint at a constant height. They also developed an optimization method using Genetic Algorithm for maximum stability and minimum energy consumption. Kim et al [9] developed an approach for dynamic bipedal walking on uneven floors including an off-line walking trajectory planning and six on-line controllers for Upright pose, landing angular momentum, landing timing, landing position, and vibration reduction and landing shock absorber. A number of researchers have presented methods employing forward kinematic approach; for example, Zhang et al [10] parameterized Denavit-Hartenberg (D-H) formulation for an off-line kinematics model with on-line adjustment ability where homogeneous transformation matrices deduce the kinematics equations. And Deng et al [11] developed a virtual environment for biped robot simulation utilized D-H for biped locomotion and dynamic balance.

Kajita et al [12] used a simple linear dynamic analysis, the 3D Linear Inverted Pendulum Mode, for real time control of a biped robot. Kajita et al [13] made use of preview control theory to compensate for the ZMP error caused by the differences between a simple model and the precise multi-body model for walking on spiral stairs. In a similar way, Suleiman et al [14] proposed an algorithm to identify a quadratic system. This

algorithm is based on using multiple walking patterns in order to identify an accurate model. The limitation of the proposed model is that when the walking trajectories are curved the ZMP behavior of the robot cannot be captured accurately.

Conventional approaches to bipedal walking did not really succeed in complicated environments particularly for real-time applications. This is mainly due to using a set of immutable kinematic equations to demonstrate the physical movements of the robot. Soft computing and artificial intelligence offer an alternative approach. Farzaneh et al [15] implemented Takagi-Sugeno (T-S) fuzzy systems for finding Finite Fourier series constants in order to overcome time consumption problem of the off-line method of trajectory generation such that the approach be applicable to real time bipedal walking planning. Luo et al [16] used a periodic function to plan the biped moving trajectory in sagittal plane. To assure short response time in trajectory tracking, a Fuzzy Sliding Mode controller including two independent controllers for positive and negative compensation was implemented. Park et al [17] used Fuzzy Logic to reduce the swing motion of the trunk and minimize disturbances. A posture control also using Fuzzy algorithm was proposed by Choi et al [18] in order to improve walking stability. Ferreira et al [19] proposed an Adaptive Neural-Fuzzy walking control of a biped robot. The implemented system was trained with expert-knowledge-driven data set of the biped motion control. Fan et al [20] developed a supervised learning Fuzzy Neural Network (FNN) for fast humanoid robot gait generation. To overcome the limitation of processing time of an eight-link biped robot dynamic equations Ferreira et al [21] proposed two alternative intelligent computing control techniques, Support Vector Regression (SVR) and a first-order Takagi-Sugeno-Kang (TSK) type Neuro-Fuzzy Network. Both methods aimed to correct robot's torso for balance in sagittal plane. The SVR and the TSK NF controllers exhibited similar stability; but, the SVR controller runs faster. Inherent complexity and imprecision in the collected environmental data led Vundavilli et al [22] to utilize soft computing methods to solve ascending and descending gait generation problems for biped robots. They developed Genetic-Neural and Genetic-Fuzzy approaches to model biped walking trajectory where Genetic Algorithm optimizes the weights and knowledge-bases in Neural Network and Fuzzy Logic Controller respectively. Cardenas-Maciel et al [23] presented a Takagi-Sugeno Fuzzy Logic Controller using a Neuro-Fuzzy learning algorithm to generate walking motions. Sabourin et al [24]

improved the stability of dynamic gait of a biped robot in existence of external disturbances with two phases control strategy. After dynamic gait sequences generation, Neural Networks is trained on joint trajectories of the reference gait. In the second step, the Neural Networks generates trajectories as learned during the first step. This approach also makes walking on irregular grounds possible. Locomotion through kinematic techniques highly depends on the amount of data. On the other hand, capturing the full range of human motions is giving infinite ways of trajectory planning. Moreover, computational performance, ease of implementation and motion smoothness are considered as main factors for the locomotion synthesis. However, these attributes may sometimes contradict each other.

In the following sections, the proposed methodology is discussed in detail. The ankle, hip, and knee joints positions at five key frames in a single gait cycle are calculated in section 2. Then, these point sets are fed into a modified architecture of the RBFNs to generalize the robot motion kinematic. A novel technique for the robot upper body trajectory planning satisfying whole structure dynamic balance is also proposed in this section. In section 3, robot motion simulation demonstrates reliability and efficiency of the proposed method. And finally, a conclusion is given in section 4.

2 Trajectory Generation Methodology

Stable bipedal walk on various surfaces demands adaptation and maintenance of stability. Adaptation is robot capability to employ different appropriate patterns of motion as the condition changes. An anthropomorphic biped robot is considered as a reference model where each leg consists of a thigh, a shank, and a foot. The under study model has six degree of freedom in sagittal plane including two DOF in the hip joint, one in each knee joint, and one in each ankle joint.

2.1 The Robot Kinematics

Bipedal walking is a periodic incident composed of Double Support Phase (DSP) which is followed by Single Support Phase (SSP). In human locomotion, the DSP time length is about 20% of a whole gait cycle [5]. In the proposed methodology, both feet and hip joints trajectories are initially derived; consequently, all the other components such as knee joint and sole of foot trajectories are determined by taking the biped robot kinematic constraints into the

consideration. Therefore, a unique walking pattern is formed by the foot and hip joints trajectories.

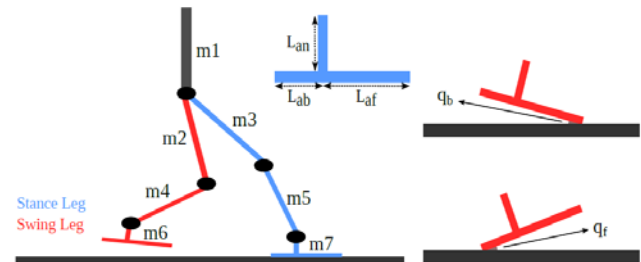


Fig. 1 The robot model specification

2.1.1 Bipedal Walking On an Ideal Flat Surface

By human gait studying during a gait cycle, a limited number of ankle and hip joints positions in both double support phase and single support phase can be identified with respect to the XZ coordinate system origin (0,0). For instance, consider ankle joint of the swinging leg during a gait cycle on a flat surface. First, the foot is in full contact with the surface (first step) then the toes of the swing foot leaving the ground with angle q_b (second step). The ankle joint would reach its maximum height (L_{ao}, H_{ao}) at the third step. When it comes to landing, heel of the swing foot touches the ground (fourth step) followed by full contact of swing foot (fifth step) with displacement of $2D_s$ along X-axis. Therefore, five key points are distinguished. The coordinates of these several points are mathematically computed through relationships of the robot's structure specifications and key assumptions. Once positions of all these featured points are first formulated and then calculated, the pattern of robot walking for the whole gait cycle can be generalized (or interpolated). The generalization is further discussed in section 2.3. Analytical set of equations or finding approximated points in between of each pair of available points are examples of other methods than interpolations. However, these mathematically complicated techniques lack desired level of accuracy and take relatively higher computation time.

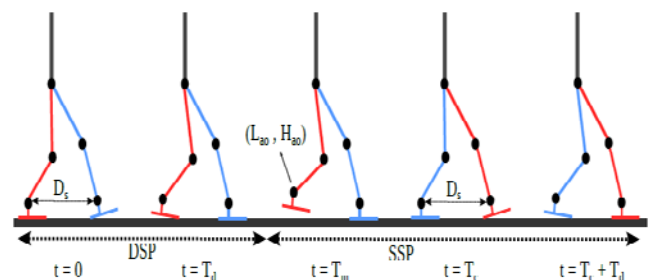


Fig. 2 Five identified key frames in a gait cycle

A robot requires trajectories for both swing and stance legs to accomplish the procedures of one single gait. Although the stance foot (ankle joint) is fixed during a gait, the knee joint position of stance leg is varying. The left and right legs in the seven-links biped model are conjunct in hip joint; therefore, a constant ankle joint position and the varying trajectory of hip joint result in a moving pattern of knee joint. By calculating all the joints positions at the key frames, joints' angles at these specified points/times in sagittal plane are determined.

In fig. 2, robot's posture at five distinguished moment during a single gait cycle is illustrated where D_s represents gait length which refers to the distance between ankle joints of swing and stance legs at initial time ($t = 0$) or at the end of a gait cycle ($t = T_c$). T_c stands for a gait cycle time (or period) and T_d is DSP duration. The swing foot obtains its maximum height at T_m . In order to facilitate adaptation to various surface modes for the biped robot, the robot's foot (ankle joint) trajectory must first be specified. During the walking cycles, the swing leg ankle joint displacements along X-axis and Z-axis are represented by $X_{a_{SW}}$ and $Z_{a_{SW}}$ respectively. Following equation formulations are extracted from trigonometric ratios of foot specifications. As an example, below the formulation of swing ankle joint position along X-axis at $t = T_d$ is illustrated.

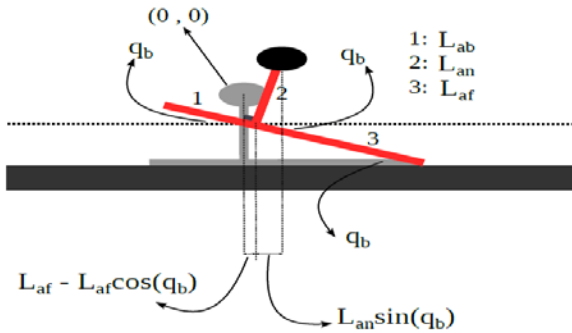


Fig. 3 Illustration of formulation

$$X_{a_{SW}}(t) = \begin{cases} 0 & t = 0 \\ L_{an} \sin q_b + L_{af}(1 - \cos q_b) & t = T_d \\ L_{ao} & t = T_m \\ 2D_s - L_{an} \sin q_f - L_{ab}(1 - \cos q_f) & t = T_c \\ 2D_s & t = T_c + T_d \end{cases} \quad (1)$$

In Eq. (1), L_{an} is the length of link connecting the ankle joint to the sole of foot, L_{af} and L_{ab} represent the rear and front parts of the foot as shown in Fig. 1. q_b and q_f are angles between the

swing foot and the ground as it leaves and touches down the ground respectively. At a point within a gait, ankle joint reaches a maximum height. L_{ao} is the position of swing ankle joint along X-axis as the joint's height reaches H_{ao} , its maximum point along Z-axis. The projected swing ankle joint positions on Z-axis in a gait time interval are parameterized in Eq. (2).

$$Z_{a_{SW}}(t) = \begin{cases} L_{an} & t = 0 \\ L_{af} \sin q_b + L_{an} \cos q_b & t = T_d \\ H_{ao} & t = T_m \\ L_{ab} \sin q_f + L_{an} \cos q_f & t = T_c \\ L_{an} & t = T_c + T_d \end{cases} \quad (2)$$

And, Eq. (3) represents sole of the swing foot angle variations. The swing foot sole is assumed to be completely in contact with the walking surface at the end of gait period ($t = T_c$) and DSP of next cycle ($t = T_c + T_d$).

$$\theta_{a_{SW}}(t) = \begin{cases} 0 & t = 0 \\ q_b & t = T_d \\ -q_f & t = T_c \\ 0 & t = T_c + T_d \end{cases} \quad (3)$$

The hip joint motion pattern in sagittal plane can be particularly identified by calculation of X_h and Z_h indicating the hip joint positions along X-axis and Z-axis respectively.

$$X_h(t) = \begin{cases} x_{ed} & t = 0 \\ D_s - x_{sd} & t = T_d \\ D_s + x_{ed} & t = T_c \end{cases} \quad (4)$$

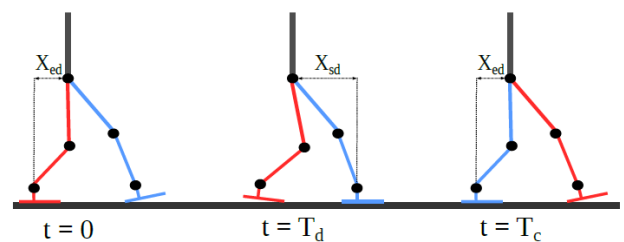


Fig. 4 x_{ed} and x_{sd} illustration

Where x_{ed} and x_{sd} illustrated in Fig. 4 represent distances from hip joint to stance ankle joint at initial and final points of the double support phase respectively. x_{ed} and x_{sd} can be manually modified in appropriate intervals as given in Eq. (5) [5].

$$\begin{cases} 0 < x_{ed} < 0.5D_s \\ 0 < x_{sd} < 0.5D_s \end{cases} \quad (5)$$

The projected hip joint positions on Z-axis for three key frames in a gait period are formulated in Eq. (6). In a gait duration, it is assumed that the hip joint obtains its maximum value with respect to the origin of the system coordinate along Z-axis, H_{max} , at the middle of single support phase and the lowest position, H_{min} , occurs at the middle of the double support phase.

$$Z_h(t) = \begin{cases} H_{min} & t = 0.5T_d \\ H_{max} & t = 0.5(T_C - T_d) \\ H_{min} & t = T_C + 0.5T_d \end{cases} \quad (6)$$

Since ankle and hip joints are connected at the knee joint through thigh and shank links in a human leg structure, calculation of the ankle and hip joints trajectories can simply result in a unique knee trajectory.

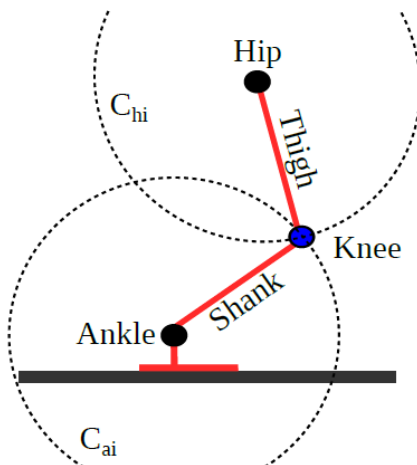


Fig. 5 The swing knee joint trajectory by intersecting circles C_{hi} and C_{ai}

In Fig. 5 illustration, the point with greater X-value of circles C_{hi} and C_{ai} intersection is the desired knee joint position in each step during a gait period. C_{hi} is a circle centered at the hip joint with radius of thigh length, and C_{ai} represents a circle with center at the swing ankle joint with radius of shank length [25]. Since the leg hardly gets completely straight up which means tangent circles do not exist, there are always two intersection points. The point with greater value along X-axis between two points of circles C_{hi} and C_{ai} intersection is selected because human leg is only bent forward.

During a gait cycle, position of stance ankle joint is constant as it has no movement. The horizontal distance of support ankle joint (X_a) from the origin of coordinate system equals to the gait length(D_S). The joint height (Z_a) is the length of the link connecting ankle joint to the foot(L_{an}).

$$\begin{cases} X_a = D_S & 0 \leq t \leq T_C \\ Z_a = L_{an} & 0 \leq t \leq T_C \end{cases} \quad (7)$$

Since the hip joint is moving forward due to swing leg motion, knee joint of stance leg adopts a varying motion pattern. The stance knee joint trajectory is identified by the aforementioned technique of intersecting circles.

By all the joints trajectories for a single gait period, the joints trajectories can be just repeated for the next cycles to proceed walking in similar ground conditions. The task of replication for achieving successive gait cycles is accomplished through trajectories replacement in turn. For instance, if the left leg is assumed to be the swing leg in the first cycle, then it is the stance leg during the second cycle and the origin of coordinate system is horizontally shifted forward by a gait length(D_S). Therefore, left leg trajectory in previous cycle is the right leg trajectory during the next consecutive gait cycle. Otherwise, if the robot encounters a different ground condition, the whole procedure of joints motion planning must be repeated such that updated trajectories adapting the new circumstance are obtained. Variation of several bipedal walk parameters such as gait length (D_S), gait period (T_C), maximum height of swing ankle joint (H_{ao}), T_m , T_d , x_{ed} , x_{sd} , q_b , and q_f can desirably modify trajectory of the whole robot body locomotion.

2.1.2 Walking on Inclined Surfaces

Similar with trajectory planning for bipedal walking on a flat surface, in a gait cycle of the robot's walking on an inclined surface, with slope of λ , several specified ankle and hip joints positions and consequently knee joint positions in both DSP and SSP can be identified. Eqs. (8)-(12) result in positions of swing ankle ($X_{a_{SW,Inc}}, Z_{a_{SW,Inc}}, \theta_{a_{SW,Inc}}$) and hip ($X_{h,Inc}, Z_{h,Inc}$) joints at the specified time.

2.1.3 Walking on Declined Surfaces

An analogous approach is employed to obtain a smooth bipedal walking pattern in the case of declined ground condition with slope of λ . Eqs. (13)-(17) return swing leg's ankle ($X_{a_{SW,Dec}}, Z_{a_{SW,Dec}}, \theta_{a_{SW,Dec}}$) and hip ($X_{h,Dec}, Z_{h,Dec}$) joints coordinates.

$$Xa_{SW,Inc} = \begin{cases} L_{ab} \cos \lambda - L_{an} \sin \lambda & t = 0 \\ L_{ab} \cos(\lambda - q_b) - L_{an} \sin(\lambda - q_b) + (L_{af} + L_{ab} - (L_{af} + L_{ab}) \cos q_b) \cos \lambda & t = T_d \\ L_{ao} \cos \lambda & t = T_m \\ 2D_S \cos \lambda - L_{an} \sin(\lambda + q_f) - L_{ab}(1 - \cos q_f) \cos \lambda & t = T_C \\ 2D_S \cos \lambda - L_{an} \sin \lambda & t = T_C + T_d \end{cases} \quad (8)$$

$$Za_{SW,Inc} = \begin{cases} L_{an} \cos \lambda + L_{ab} \sin \lambda & t = 0 \\ Xa_{SW,Inc}(T_d) \tan \lambda + L_{an} \cos(\lambda - q_b) + (L_{af} \cos(\lambda - q_b) - L_{an} \sin(\lambda - q_b)) \tan \lambda - L_{af} \sin(\lambda - q_b) & t = T_d \\ L_{ao} \sin \lambda + H_{ao} & t = T_m \\ L_{an} \sin(\lambda + q_f) + L_{ab} \sin(\lambda + q_f) + (2D_S - L_{ab}) \sin \lambda & t = T_C \\ L_{an} \cos \lambda + 2D_S \sin \lambda & t = T_C + T_d \end{cases} \quad (9)$$

$$\theta a_{SW}(t) = \begin{cases} -\lambda & t = 0 \\ -\lambda + q_b & t = T_d \\ -\lambda - q_f & t = T_C \\ -\lambda & t = T_C + T_d \end{cases} \quad (10) \quad X_{h,Inc}(t) = \begin{cases} x_{ed} & t = 0 \\ D_S \cos \lambda - x_{sd} & t = T_d \\ D_S \cos \lambda + x_{ed} & t = T_C \end{cases} \quad (11)$$

$$Z_{h,Inc}(t) = \begin{cases} H_{min} + D_S \sin \lambda & t = 0.5T_d \\ H_{max} + D_S \sin \lambda & t = 0.5(T_C - T_d) \\ H_{min} + D_S \sin \lambda & t = T_C + 0.5T_d \end{cases} \quad (12)$$

$$Xa_{SW,Dec} = \begin{cases} L_{ab} \cos \lambda + L_{an} \sin \lambda & t = 0 \\ L_{ab} \cos(\lambda + q_b) - L_{an} \sin(\lambda + q_b) + (L_{af} + L_{ab} - (L_{af} + L_{ab}) \cos q_b) \cos \lambda & t = T_d \\ L_{ao} \cos \lambda & t = T_m \\ 2D_S \cos \lambda - L_{an} \sin(q_f - \lambda) - L_{ab}(1 - \cos q_f) \cos \lambda & t = T_C \\ 2D_S \cos \lambda - L_{an} \sin \lambda & t = T_C + T_d \end{cases} \quad (13)$$

$$Za_{SW,Dec} = \begin{cases} L_{an} \cos \lambda + L_{ab} \sin \lambda & t = 0 \\ Xa_{SW,Inc}(T_d) \tan \lambda + L_{an} \cos(\lambda + q_b) + (L_{af} \cos(\lambda - q_b) - L_{an} \sin(\lambda - q_b)) \tan \lambda - L_{af} \sin(\lambda - q_b) & t = T_d \\ H_{ao} & t = T_m \\ L_{an} \sin(\lambda + q_f) + L_{ab} \sin(\lambda + q_f) + (2D_S - L_{ab}) \sin \lambda & t = T_C \\ L_{an} \cos \lambda - 2D_S \sin \lambda & t = T_C + T_d \end{cases} \quad (14)$$

$$\theta a_{SW,Dec} = \begin{cases} \lambda & t = 0 \\ \lambda + q_b & t = T_d \\ \lambda - q_f & t = T_C \\ \lambda & t = T_C + T_d \end{cases} \quad (15)$$

$$Z_{h,Dec} = \begin{cases} H_{min} & t = 0.5T_d \\ H_{max} - D_S \sin \lambda & t = 0.5(T_C - T_d) \\ H_{min} - D_S \sin \lambda & t = T_C + 0.5T_d \end{cases} \quad (17)$$

$$X_{h,Dec} = \begin{cases} x_{ed} & t = 0 \\ D_S \cos \lambda - x_{sd} & t = T_d \\ D_S \cos \lambda + x_{ed} & t = T_C \end{cases} \quad (16)$$

2.1.4 Walking Up Stairs

In pattern planning for the robot walking on stairs, fig. 6, either going up or down stairs, the gait length (D_S) is set to stair depth. Eqs. (18)-(22) describe swing leg's ankle ($Xa_{SW,Ustr}, Za_{SW,Ustr}, \theta a_{SW,Ustr}$) and hip ($X_{h,Ustr}, Z_{h,Ustr}$) joints positions at key time frames during a gait period along the X-axis

and the Z-axis respectively when the biped robot is going up stairs.

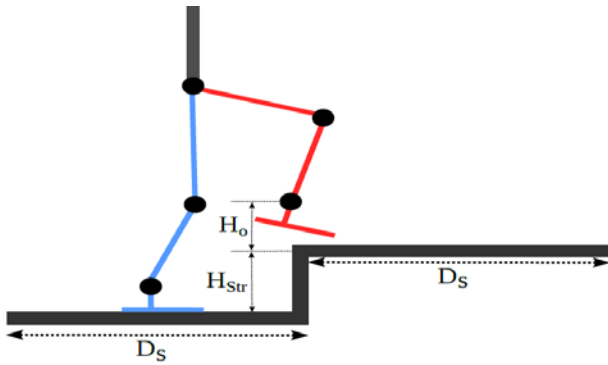


Fig. 6 Characteristics of walking on stairs

$$Xa_{SW,Ustr}(t) = \begin{cases} 0 & t = 0 \\ L_{an} \sin q_b + L_{af}(1 - \cos q_b) & t = T_d \\ L_{ao} & t = T_m \\ 2D_s - L_{an} \sin q_f - L_{ab}(1 - \cos q_f) & t = T_C \\ 2D_s & t = T_C + T_d \end{cases} \quad (18)$$

$$Za_{SW,Ustr}(t) = \begin{cases} L_{an} & t = 0 \\ L_{af} \sin q_b + L_{an} \cos q_b & t = T_d \\ H_o + H_{Str} & t = T_m \\ H_{Str} + L_{ab} \sin q_f + L_{an} \cos q_f & t = T_C \\ H_{Str} + L_{an} & t = T_C + T_d \end{cases} \quad (19)$$

$$\theta a_{SW,Ustr}(t) = \begin{cases} 0 & t = 0 \\ q_b & t = T_d \\ -q_f & t = T_C \\ 0 & t = T_C + T_d \end{cases} \quad (20)$$

$$X_{h,Ustr}(t) = \begin{cases} x_{ed} & t = 0 \\ D_s - x_{sd} & t = T_d \\ D_s + x_{ed} & t = T_C \end{cases} \quad (21)$$

$$Z_{h,Ustr}(t) = \begin{cases} H_{min} & t = 0.5T_d \\ H_{max} & t = 0.5(T_C - T_d) \\ H_{min} & t = T_C + 0.5T_d \end{cases} \quad (22)$$

2.1.5 Walking Down Stairs

Eqs. (23)-(27) describe swing leg's ankle ($Xa_{SW,Dstr}, Za_{SW,Dstr}, \theta a_{SW,Dstr}$) and hip ($X_{h,Dstr}, Z_{h,Dstr}$) joints positions at specified time steps for walking down stairs.

$$Xa_{SW,Dstr}(t) = \begin{cases} 0 & t = 0 \\ L_{an} \sin q_b + L_{af}(1 - \cos q_b) & t = T_d \\ L_{ao} & t = T_m \\ 2D_s + L_{an} \sin q_f + L_{af}(1 - \cos q_f) & t = T_C \\ 2D_s & t = T_C + T_d \end{cases} \quad (23)$$

$$Za_{SW,Dstr}(t) = \begin{cases} L_{an} + H_{Str} & t = 0 \\ L_{af} \sin q_b + L_{an} \cos q_b + H_{Str} & t = T_d \\ H_{Str} & t = T_m \\ L_{af} \sin q_f + L_{an} \cos q_f - H_{Str} & t = T_C \\ L_{an} - H_{Str} & t = T_C + T_d \end{cases} \quad (24)$$

$$\theta a_{SW,Dstr}(t) = \begin{cases} 0 & t = 0 \\ q_b & t = T_d \\ q_f & t = T_C \\ 0 & t = T_C + T_d \end{cases} \quad (25)$$

$$X_{h,Dstr}(t) = \begin{cases} x_{ed} & t = 0 \\ D_s - x_{sd} & t = T_d \\ D_s + x_{ed} & t = T_C \end{cases} \quad (26)$$

$$Z_{h,Dstr}(t) = \begin{cases} H_{min} & t = 0.5T_d \\ H_{max} & t = 0.5(T_C - T_d) \\ H_{min} - H_{Str} & t = T_C + 0.5T_d \end{cases} \quad (27)$$

2.2 A Non-Conventional Generalization

ANNs are able to model the non-linear relationships between several sets of model inputs and their equivalent outputs. ANNs are organized in several layers of interconnected processing nodes working together to transform the inputs to the outputs of the model. ANNs are appropriate for modeling complex systems whose parameters relationships are highly complicated to be identified.

According to section 2.1 formulations, time (t) is assumed as the input variable for the swing ankle joint [$Xa_{SW}(t), Za_{SW}(t), \theta a_{SW}(t)$] and the hip joint [$X_h(t), Z_h(t)$] characteristic parameters. When the number of outputs is more than the number of inputs, ANNs return infinite mapping paths. Besides, efficient error propagation cannot take place where the output layer neurons are more than the number of inputs. In order to improve the generalization power of ANNs in such cases, a new method is proposed in this dissertation. A Radial Basis Function Network has been utilized in this method which performs more fittingly on limited

number of input/output data sets comparing with the Feed Forward Back Propagation Network.



Fig. 7 An Artificial Neural Network with input/output sets

The output variables are functions of inputs of the system, fig. 7.

$$\begin{cases} y_1 = f_1(x_1, x_2, x_3, \dots, x_n) \\ \vdots \\ y_2 = f_2(x_1, x_2, x_3, \dots, x_n) \end{cases} \quad x \in \mathfrak{R}^n, y \in \mathfrak{R}^m \quad (28)$$

When $m > n$ there are infinite solutions for the system. In other words, the ANN is not able to properly find a unique solution for the system. If the number of outputs equals to the number of inputs ($m = n$) there is just one solution for the system. If $m < n$, there may exist one approximate solution for the system.

For ankle joint, position in sagittal plane is identified by $[Xa_{sw}(t), Za_{sw}(t), \theta a_{sw}(t)]$ where $Xa_{sw}(t)$ and $Za_{sw}(t)$ represent its horizontal and vertical positions respectively and $\theta a_{sw}(t)$ stands for sole of the swing foot angle at each time step, fig. 8. First step for setting up an ANN is to identify the training data set which includes specified times (t) as the input $Xa_{sw}(t), Za_{sw}(t),$ and $\theta a_{sw}(t)$ as outputs.

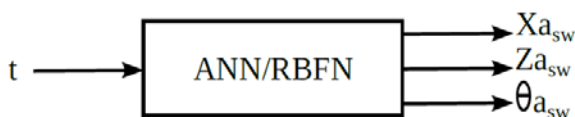


Fig. 8 The ANN initial structure for swing ankle joint generalization

Therefore, to supply the ANN requirements for situation where number of inputs is greater than or equal to the number of outputs ($n \geq m$), the proposed method is to implement a multi phase ANN structure. In this technique, as illustrated in Fig. 9, $Xa_{sw}(t), Za_{sw}(t),$ and $\theta a_{sw}(t)$ behaviors in time domain are obtained through two phases.

Each phase encompasses an Artificial Neural Network with ($m = n$) or ($n > m$). Since the sole of the foot ankle has the least available input/output data set, in the first phase $\theta a_{sw}(t)$ is generalized. Second phase which is fed by the first ANN's input

and output sets interpolates vertical and horizontal ankle joint behaviors.

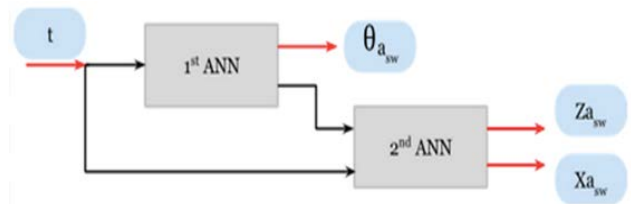


Fig. 9 Two-phases ANN structure for swing ankle joint generalization

In the Radial Basis Function Network architecture including inputs, radial basis layer and output layer, number of neurons in the output layer equals to the number of the output variables which is one and two for first and second phases respectively. Since the number of neurons in the radial basis layer is determined automatically during the training process, it is not required to initially be specified. The radial basis function as the transfer function of the single hidden layer is also pre-specified for the Radial Basis Function Networks. Besides, the spread of radial basis function should be wide enough to let the radial basis neurons sufficiently overlap. The Levenberg-Marquardt algorithm is set as the learning method. Moreover, the network goal, the mean squared error performance function, can be adjusted according to the desired accuracy (i.e. **MSE = 10⁻⁵**).

Once the network architecture design is accomplished, the training sets are fed into the RBFNs. The numbers of the training sets for first and second RBFNs are four and five respectively. After the network is trained, the ankle joint position at any arbitrary time in the gait cycle is available.

So far, the ankle joint motion pattern is available through training a function based on limited number of sets of data where it can be assessed for smoothness, shape and being human-like motion. If the Radial Basis Function Network does not return a proper and satisfactory graph, all the steps would be retaken with new network characteristics so that a desirable pattern is obtained. Comparing with conventional interpolation methods where a non-adjustable result is returned, this can be counted as a valuable advantage of ANNs. It should also be pointed out that RBFN is more effectively dealing with generalization of multidimensional scattered data.

On the other hand, it might be questioned how the network is trained only on several data sets, four or five sets, and why a small number of data sets is sufficient to train the RBFN properly. The unique

characteristics of this specific type of Artificial Neural Network along with utilizing a radial basis function, in this research Gaussian function, in the hidden layer neurons as the activation function ease the training in circumstances with small number of input/output data sets.

For the hip joint generalization, since there are two outputs, a two-phase ANN structure will return desirable hip trajectory. As indicated in Fig. 10, in the first RBFN, specified set of time steps is the input set and the horizontal ankle joint positions (X_h) stands for the output set. Second phase fed by the first ANN's input and output is aimed to generalize vertical ankle joint behavior (Z_h).

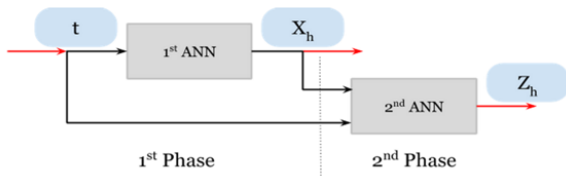


Fig. 10 The multi-phase ANN architecture for the hip joint motion planning

2.3 Biped robot dynamic investigation

The biped robot dynamic is defined as the relationships between applied forces and the resulted accelerations. In this section, a balance maintenance method applicable to real-time biped robot's tasks is introduced. The technique for the robot stability locates robot's trunk such that the ZMP is kept within the support area. This technique utilizes Linear Inverted Pendulum Model [12] with a massless rod that the whole robot structure is replaced with a single rigid body located at the COM with robot mass. In addition, the desired ZMP is pre-specified for the most stable situation placed at center of the polygon of support where it has the maximum distances from the support area margins. Therefore, the position of the robot's trunk is obtained for each single gait step. Prior proceeding to the next gait step, ZMP position is investigated with respect to the new polygon of support. If ZMP is still within the support area, the previous trunk position is kept; otherwise, the whole procedure of obtaining new trunk location is repeated under new constraints.

In Fig. 11 illustration, m_i stands for mass of i^{th} linkage and M represents the total center of mass. ZMP specifies a point on the ground ($Z_{ZMP} = 0$) where the net moment of the inertial and the gravity forces has no component along the X-axis.

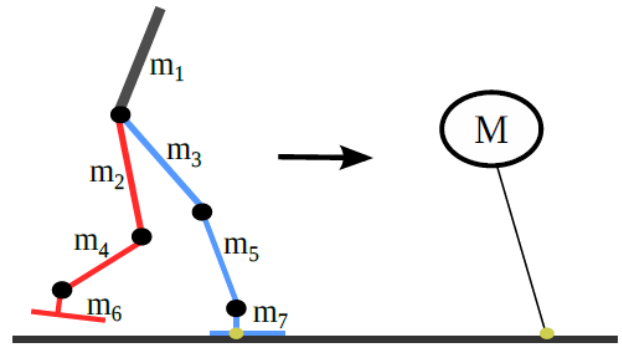


Fig. 11 Inverted pendulum model of a biped robot

The dynamics and the concept of ZMP are applied on the inverted pendulum in Eqs. (29) and (30) [13].

$$\tau = -Mg(x_{COM} - X_{ZMP}) + M\ddot{x}_{COM} \quad (29)$$

Since torque, $\tau = 0$ for ZMP, then:

$$X_{ZMP} = x_{COM} - \frac{\ddot{x}_{COM}}{g} z_{COM} \quad (30)$$

Stability margins along X-axis are defined as the area between the two feet for the double support phase and the space under the contact foot when just one foot touches the ground.

$$\left\{ \begin{array}{l} \left\{ \begin{array}{l} X_{PoS}^{Low} = X_{1,SW}(t) \\ X_{PoS}^{Up} = X_3 \end{array} \right. \quad t = 0 \\ \left\{ \begin{array}{l} X_{PoS}^{Low} = X_{3,SW}(t) \\ X_{PoS}^{Up} = X_3 \end{array} \right. \quad 0 < t \leq T_d \\ \left\{ \begin{array}{l} X_{PoS}^{Low} = X_1 \\ X_{PoS}^{Up} = X_3 \end{array} \right. \quad T_d < t < T_C \\ \left\{ \begin{array}{l} X_{PoS}^{Low} = X_1 \\ X_{PoS}^{Up} = X_{1,SW} \end{array} \right. \quad t = T_C \end{array} \right. \quad (31)$$

In all intervals identified in Eq. (31), desired ZMP is obtained through average of the lower and upper boundary points. By replacing the total center of mass which is a function of the trunk position along X-axis calculated in Eq. (30), ZMP is expressed in the term of trunk position.

$$X_{ZMP} = x_{COM}(X_T) - \frac{\ddot{x}_{COM}}{g} z_{COM} \quad (32)$$

At the first gait step, the ZMP along the X-axis is set as the middle point of the specified stability interval, fig. 12. For the next gait steps, if the pre-

specified ZMP is still within the new support area, the previous trunk position is kept; otherwise, computation of new trunk location is repeated under new constraints [26].

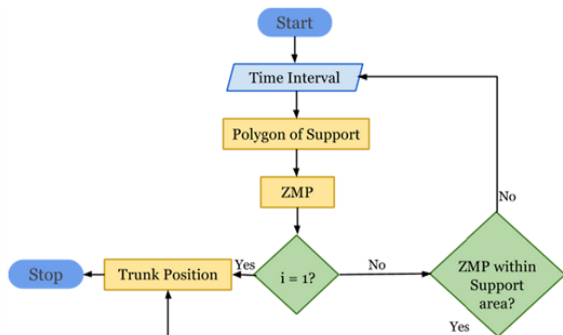


Fig. 12 The trunk trajectory planning algorithm

3 Results and discussion

The correlation between the robot's joints specifications and walking patterns is demonstrated through the simulation developed in MATLAB. Fig. 13 depicts the robot's body postures in sagittal (XZ) plane during two gait cycles with the robot's gait specifications given in Table 3.

Table 1 Constant parameters

		Length (cm)
Trunk Length		55
Thigh Length		47
Shank Length		42
Foot specifications	L_{an}	10
	L_{ab}	7
	L_{af}	15

Table 2 links concentrated masses

Percentages of total robot mass	Quantity	
Trunk (m_1)	43.02	1
Thigh (m_2, m_3)	14.47	2
Shank (m_4, m_5)	4.57	2
Foot (m_6, m_7)	1.33	2

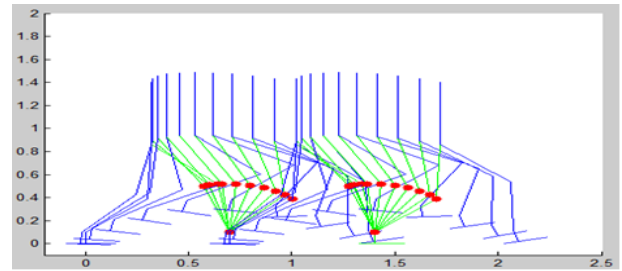


Fig. 13 The biped robot walking trajectory on flat ground condition

Table 3 The robot's gait specifications

D_S	q_b	q_f	L_{ao}	H_{ao}	x_{sd}	x_{ed}
70	$\frac{\pi}{12}$	$\frac{\pi}{12}$	30	30	35	32
cm			cm	cm	cm	cm

Fig. 14 represents a closer view of robot walking during a single gait with applied dynamical considerations. Fig. 15 – 18 illustrate joints and sole of foot motion patterns in sagittal (XZ) plane.

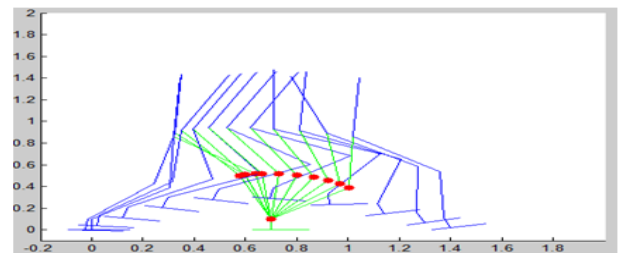


Fig. 14 Robot walking during a single gait with applied dynamical considerations

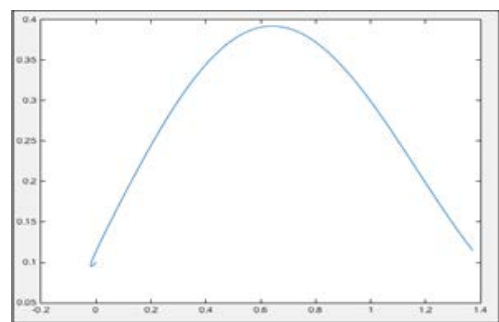


Fig. 15 Ankle joint motion pattern

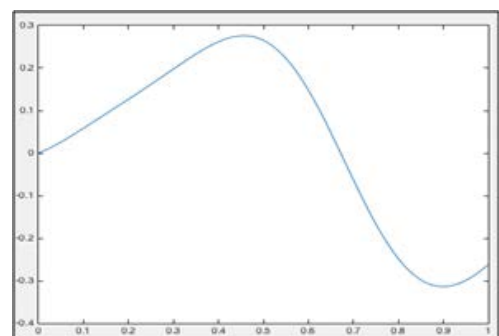


Fig. 16 Sole of the swing foot angle

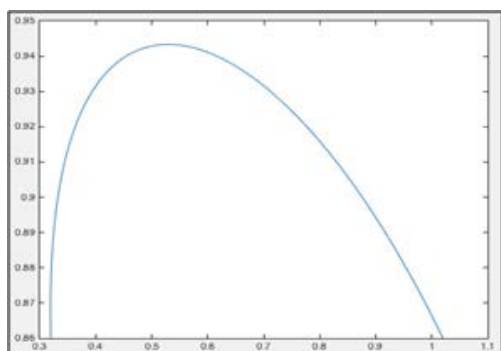


Fig. 17 Hip joint trajectory

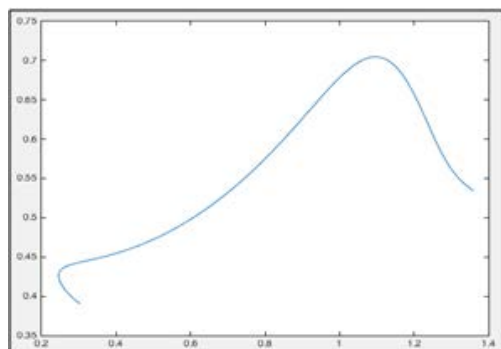


Fig. 18 The swing leg's knee joint

cycle where in Single Support Phase has a constant area due to the fact that in this phase only the support foot is in complete contact with the surface.

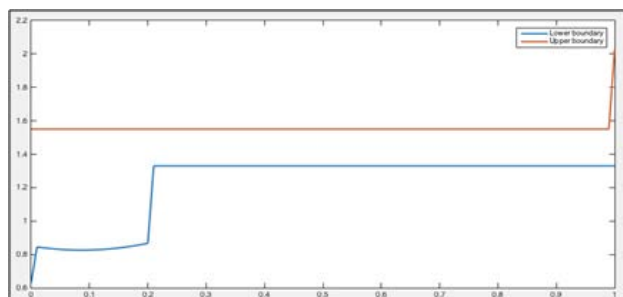


Fig. 19 Support area in the first gait cycle

The walking pattern simulation has also been developed with spline interpolation method. Following figure, fig. 20, depicts stick diagram of a biped robot utilizing a conventional interpolation method.

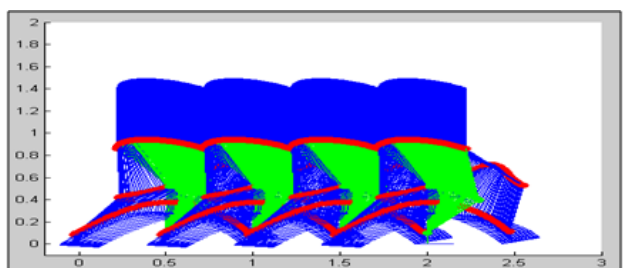


Fig. 20 Trajectory by spline interpolation

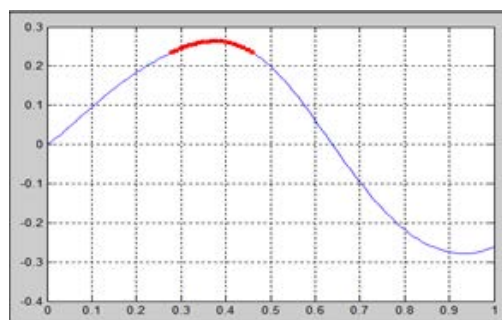


Fig. 21 Sole of the foot angle by RBFN

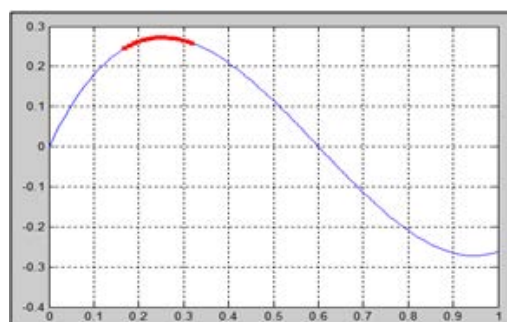


Fig. 22 Sole of the foot angle by Spline

Fig. 21 illustration represents the foot's angle behavior obtained through RBFN during a single gait cycle and its counterpart with similar applied specifications resulted from spline interpolation methodology in Fig. 22. At first glimpse, it is revealed that RBFN returns a smoother graph which is more desirable for mimicking human walking; however, RBFN flexibility in pattern modifications on same data sets is a more significant advantage.

Ground conditions with positive or negative slope are of very often situations that a robot performing in a human-acting environment faces with. Fig. 23 depicts the robot's motion trajectory in three gait cycles with a fixed gait step $D_s = 40$ cm when it is walking downhill. The biped robot's gait specifications in Fig. 23 illustration are listed in table 4. Joints and sole of foot motion patterns on XZ plane are depicted in fig. 24 – 27.

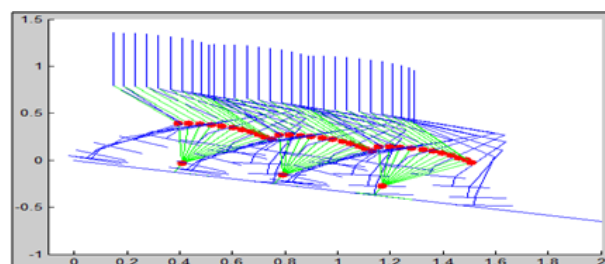


Fig. 23 Downhill walking trajectory

Table 4 Robot's gait specifications for declined surface

D_s	q_b	λ	q_f	L_{ao}	H_{ao}	x_{sd}	x_{ed}
40 cm	$\frac{\pi}{12}$	$\frac{\pi}{10}$	$\frac{\pi}{12}$	30 cm	30 cm	15 cm	15 cm

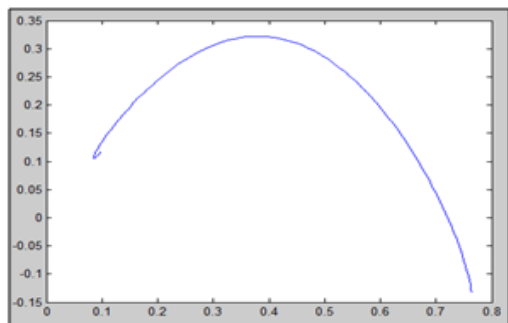


Fig. 24 Ankle pattern on declined surface

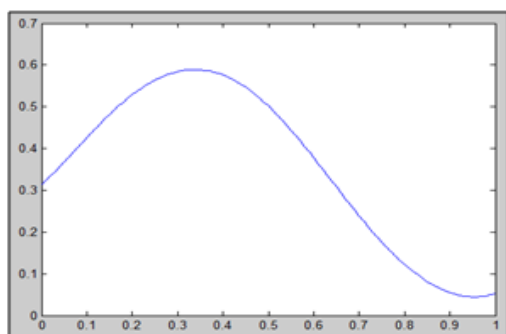


Fig.25 Sole of the foot angle

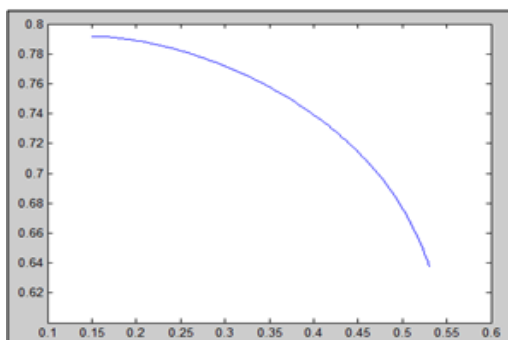


Fig. 26 Hip joint pattern

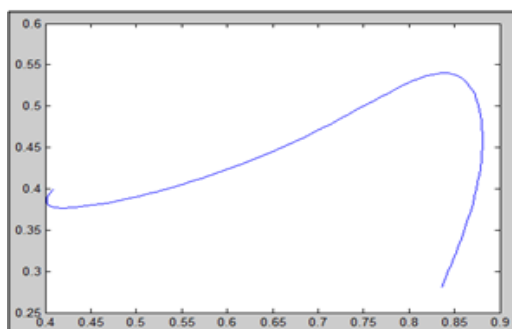


Fig. 27 Knee joint pattern

Fig. 28 depicts the robot's motion trajectory in three gait cycles with a fixed gait step $D_s = 50$ cm when it is walking up hill.

Table 5 Robot's gait specifications for inclined surface

D_s	q_b	λ	q_f	L_{ao}	H_{ao}	x_{sd}	x_{ed}
50 cm	$\frac{\pi}{12}$	$\frac{\pi}{10}$	$\frac{\pi}{12}$	30 cm	30 cm	25 cm	22 cm

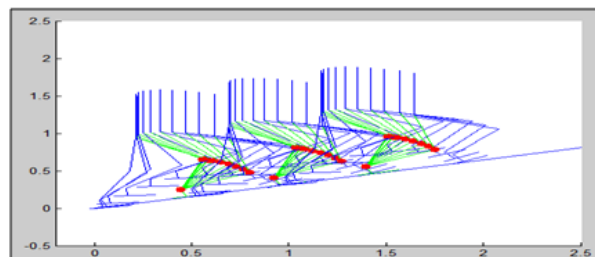


Fig. 28 Up-hill walking trajectory

Fig. 29 and fig. 30 depict the robot's motion trajectory in five and four gait cycles with a fixed gait step $D_s = 70$ cm and a smaller gait step of $D_s = 50$ cm respectively when it is walking down stairs.

Table 6 Robot's gait specifications for walking down stairs

q_b	q_f	L_{ao}	H_{ao}	x_{sd}	x_{ed}
$\frac{\pi}{12}$	$\frac{\pi}{12}$	30 cm	30 cm	25 cm	22 cm

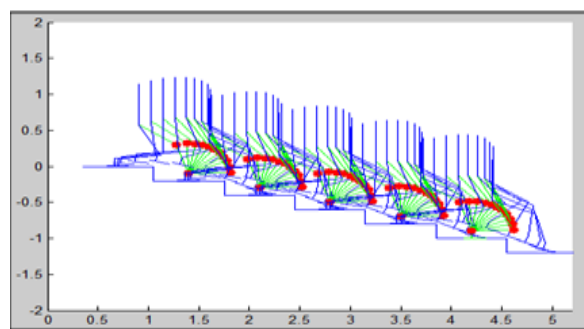


Fig. 29 Walking down stairs trajectory

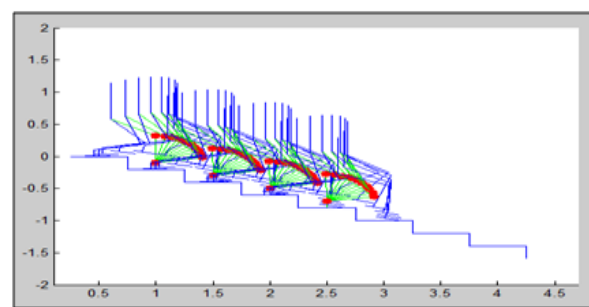


Fig. 30 Walking down stairs with a smaller step size

Table 7 Ankle RBFNs specifications for walking down stairs

	Neurons	MSE		Neurons	MSE
	Ankle pattern along X-axis	0		0.40811	Ankle pattern along Z-axis
2		0.00785	2	0.00023	
3		3.2e-05	3	4.7e-09	
4		1.6e-29	4	1.3e-34	
5		7.9e-29	5	1.2e-32	

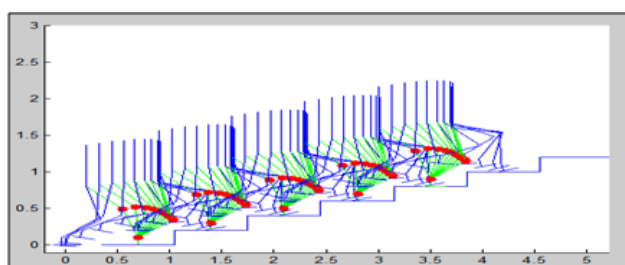


Fig. 31 Biped robot's walking upstairs trajectory

Fig. 32 represents the network training performance of the hip motion along Z-axis. As represented the desired error rate is zero; however, the network lowest overall Mean Square Error is $3.977e^{-30}$ with three epochs.

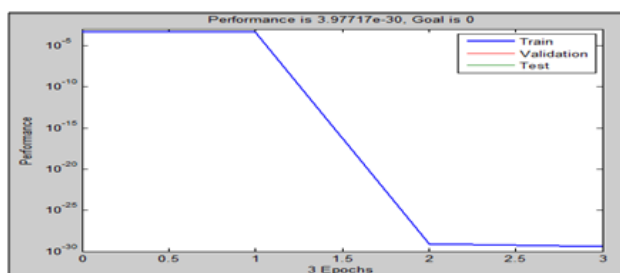


Fig. 32 RBFN performance diagram

4 Conclusions

The study on biped robot consisted of rigid bodies connected with actuated joints is supposed to mimic human walking pattern on various ground conditions. In this paper it is assumed that bipedal walking to be a periodic pattern of Single Support Phase followed by Double Support Phase. The proposed methodology divided in two parts, planning robot trajectory and dynamic stability

investigation, facilitates a scalable gait with characteristic parameters. The bipedal walking trajectory which is adaptive to the ground condition is computed by limited numbers of breakpoints in both stable and unstable phases. Consequently, positions of ankle, hip, and knee joints are derived for a seven link biped robot. In order to satisfy the smoothness of walking pattern as well as efficiency of the computation algorithm, ANNs using a RBFN to generalize a curve on derived key points are implemented. Despite other previously developed approaches addressed earlier; in this paper the ANNs are not “canned” and offer a higher level of flexibility. That is, by feeding a data set to a conventional interpolation method, yields a particular “curve”. Though, changing ANNs parameters brings a non-identical trajectory.

For dynamic stability, the ZMP for the most stable condition in a determined polygon of support is calculated. Then, to update the trunk motion to compensate for lower limb movement, a Linear Inverted Pendulum Model and ZMP criterion are employed to attain upper body trajectory satisfying whole robot walking dynamic stability.

The main contributions of this paper include: a non-conventional methodology for efficient computation of robot walking trajectory applicable to on-line tasks; a human-like bipedal walking pattern planning adaptive to various ground conditions; a novel technique based on RBFNs to enhance performance of conventional numerical methods; and a simplified dynamical walking stability investigation.

Acknowledgement

This paper research has been supported by a grant (No: 155147-2013) from the Natural Sciences and Engineering Research Council of Canada (NSERC).

References:

- [1] Miller III, W. Thomas.: Real-time neural network control of a biped walking robot. Control Systems, IEEE 14, no. 1, 41-48 (1994)
- [2] Hirai, Kazuo, Masato Hirose, Yuji Haikawa, Toru Takenaka.: The development of Honda humanoid robot. Robotics and Automation, vol. 2, 1321-1326. IEEE (1998)
- [3] Yamaguchi, Jin'ichi, Eiji Soga, Sadatoshi Inoue, Atsuo Takanishi.: Development of a bipedal humanoid robot-control method of whole body cooperative dynamic biped walking. Robotics and Automation, vol. 1, 368-374. IEEE (1999)
- [4] Vukobratovic, Miomir, A. A. Frank, Davor Juricic.: On the stability of biped locomotion.

- IEEE Transactions on Biomedical Engineering 1, no. BME-17 25-36 (1970)
- [5] Huang, Qiang, Kazuhito Yokoi, Shuuji Kajita, Kenji Kaneko, Hirohiko Arai, Noriho Koyachi, Kazuo Tanie.: Planning walking patterns for a biped robot. *Robotics and Automation, IEEE Transactions on* 17, no. 3 280-289 (2001)
- [6] Mousavi, Peiman Naseradin, Ahmad Bagheri.: Mathematical simulation of a seven link biped robot on various surfaces and ZMP considerations. *Applied Mathematical Modelling* 31, no. 1 18-37 (2007)
- [7] Mousavi, Peiman Naseradin, C. Nataraj, Ahmad Bagheri, Mahdi Alizadeh Entezari.: Mathematical simulation of combined trajectory paths of a seven link biped robot. *Applied Mathematical Modelling* 32, no. 7 1445-1462 (2008)
- [8] Fattah, A., A. Fakhari.: Trajectory planning of walking with different step lengths of a seven-link biped robot. *ASME International Design Engineering Technical Conferences and Computers and Information in Engineering Conference*, pp. 1361-1369 (2010)
- [9] Kim, Jung-Yup, Ill-Woo Park, Jun-Ho Oh.: Walking control algorithm of biped humanoid robot on uneven and inclined floor. *Journal of Intelligent and Robotic Systems* 48, no. 4 457-484 (2007)
- [10] Zhang, Qiushi, Dandan Chen, Hongmei Li.: A Gait planning method for biped Heel-And-Toe robot. *Energy Procedia* 16 1799-1805 (2012)
- [11] Deng, Xing-qiao, Jin-ge Wang, Zhong-fan Xiang.: The Simulation Analysis of Humanoid Robot Based on Dynamics and Kinematics. *Intelligent Robotics and Applications*, 93-100. Springer Berlin Heidelberg (2008)
- [12] Kajita, Shuuji, Fumiio Kanehiro, Kenji Kaneko, Kiyosli Fujiwara, Kazuliito Yokoi, Hirohisa Hirukawa.: A realtime pattern generator for biped walking. *Robotics and Automation ICRA'02 vol. 1*, 31-37. IEEE (2002)
- [13] Kajita, Shuuji, Fumio Kanehiro, Kenji Kaneko, Kiyoshi Fujiwara, Kensuke Harada, Kazuhito Yokoi, Hirohisa Hirukawa.: Biped walking pattern generation by using preview control of zero-moment point. *Robotics and Automation ICRA'03 vol. 2*, 1620-1626. IEEE (2003)
- [14] Suleiman, Wael, Fumio Kanehiro, Kanako Miura, Eiichi Yoshida.: Enhancing zero moment point-based control model: system identification approach. *Advanced Robotics* 25, no. 3-4 427-446 (2011)
- [15] Farzaneh, Yadollah, Alireza Akbarzadeh, Ali Akbar Akbari.: Online bio-inspired trajectory generation of seven-link biped robot based on t-s fuzzy system. *Applied Soft Computing* 14 167-180 (2014)
- [16] Luo, Ren C., Chiung-wei Tzeng, Po-zen Cheng, Kao-wei Lee.: Trajectory-tracking of nonlinear biped robot system based on adaptive fuzzy sliding mode control. *Industrial Electronics Society* 33 2789-2794. IEEE (2007)
- [17] Park, Jong Hyeon, Hoam Chung.: ZMP compensation by online trajectory generation for biped robots. *Systems, Man, and Cybernetics, SMC'99 vol. 4*, 960-965. IEEE (1999)
- [18] Choi, Kyu-Cheon, Hyun-Jeong Lee, Hyun-Jeong Lee.: Fuzzy posture control for biped walking robot based on force sensor for ZMP. *SICE-ICASE*, 1185-1189. IEEE (2006)
- [19] Ferreira, Joao P., Tito G. Amaral, Vítor Fernão Pires, Manuel M. Crisostomo, Paulo Coimbra.: A neural-fuzzy walking control of an autonomous biped robot. *Automation Congress vol. 15*, 253-258. IEEE (2004)
- [20] Fan, Shouwen, Min Sun, Mingquan Shi.: Real-time gait generation for humanoid robot based on fuzzy neural networks. *Natural Computation, ICNC 3 vol. 2*, 343-348. IEEE (2007)
- [21] Ferreira, Joao P., Manuel M. Crisostomo.: SVR versus neural-fuzzy network controllers for the sagittal balance of a biped robot. *Neural Networks* 20, no. 12 1885-1897 IEEE (2009)
- [22] Vundavilli, Pandu Ranga, Dilip Kumar Pratihari.: Soft computing-based gait planners for a dynamically balanced biped robot negotiating sloping surfaces. *Applied Soft Computing* 9, no. 1 191-208. (2009)
- [23] Cardenas-Maciél, Selene L., Oscar Castillo, Luis T. Aguilar, Juan R. Castro.: A TS Fuzzy Logic Controller for biped robot walking based on adaptive network fuzzy inference system. *Neural Networks (IJCNN)* 1-8. IEEE (2010)
- [24] Sabourin, Christophe, Olivier Bruneau.: Robustness of the dynamic walk of a biped robot subjected to disturbing external forces by using CMAC neural networks. *Robotics and Autonomous Systems* 51, no. 2 81-99 (2005)
- [25] B. Nikbin, M.R. Ranjbar, B. Shafiee Sarjaz, H. Shah-Hosseini.: Biped Robot Walking using Particle Swarm Optimization. *Soft Computing in Industrial Applications WSC16* (2011).
- [26] Mohammadreza Ranjbar, Rene V. Mayorga.: Trajectory Planning for Robot Bipedal Walking Using Radial Basis Functions Networks. *Neural Networks* 15. *Advances in Computational Intelligence* 69-75. (2015)